Integration of colloidal silicon nanocrystals on metal electrodes in single-electron transistor

Yasuhiro Higashikawa, Yasuo Azuma, Yutaka Majima, Shinya Kano, and Minoru Fujii

Citation: Appl. Phys. Lett. **109**, 213104 (2016); doi: 10.1063/1.4968583
View online: http://dx.doi.org/10.1063/1.4968583
View Table of Contents: http://aip.scitation.org/toc/apl/109/21
Published by the American Institute of Physics

Integration of colloidal silicon nanocrystals on metal electrodes in single-electron transistor

Yasuhiro Higashikawa,[1] Yasuo Azuma,[2] Yutaka Majima,[2] Shinya Kano,[1,a)] and Minoru Fujii[1]
[1]*Department of Electrical and Electronic Engineering, Graduate School of Engineering, Kobe University, Kobe 657-8501, Japan*
[2]*Laboratory for Materials and Structures, Tokyo Institute of Technology, Yokohama 226-8503, Japan*

(Received 7 September 2016; accepted 11 November 2016; published online 22 November 2016)

We develop a facile process to integrate colloidal silicon nanocrystals (Si NCs) with metal electrodes in a single-electron transistor by self-assembly. Gold (Au) surface is modified by an amine-terminated self-assembled monolayer to have a positive potential. All-inorganic boron (B) and phosphorus (P) codoped Si NCs, with a negative surface potential and size-controllability, are selectively adsorbed on an amine-terminated Au surface by electrostatic attraction. We demonstrate the fabrication of SETs consisting of electroless-plated Au nanogap electrodes and codoped Si NCs using this process and observation of clear Coulomb diamonds at 9 K. *Published by AIP Publishing.*
[http://dx.doi.org/10.1063/1.4968583]

Colloidal semiconductor nanocrystals (NCs) have been intensively studied because their optical and electronic properties are largely modified by quantum confinement with respect to the bulk counterparts.[1] They can be a precursor for the development of optoelectronic devices by the solution-based processes.[2] High-performance field-effect transistors,[3,4] photovoltaics,[5,6] and light-emitting diodes[7,8] have been developed by using the spin-coated colloidal semiconductor NCs.

One of the promising applications of colloidal NCs is a single-electron transistor (SET), which can be used in several kinds of nanodevices such as reconfigurable Boolean logic,[9,10] single-electron charge sensor,[11,12] and single-electron pump.[13] Since the operational temperature of SETs is strongly related to the size of a Coulomb island, size-regulated NCs are potentially very attractive as a material for a Coulomb island.[14–16] For this application, single-nanometer NCs are required to be immobilized between the nanogap electrodes, which is not possible by conventional semiconductor technology. Self-assembly with the assistance of organic molecules is an effective route to immobilize NCs in the nanogap electrodes.

The most widely used NC material in SETs is gold (Au). By using the well-established process utilizing the alkanedithiol molecules, Au NCs can be bound onto metal electrodes.[17–20] Furthermore, colloidal II-VI semiconductor NCs such as cadmium selenide (CdSe) NCs[21] are used for the fabrication of SETs and a light-emitting SET.[22] However, NCs composed of these heavy-metal elements are not compatible with the existing complementary metal-oxide-semiconductor (CMOS) technology. Integration of SETs with these colloidal NCs in the existing electronic devices is not straightforward.

In this work, we develop a process to integrate colloidal silicon (Si) NCs with SETs. Si is an environmental-friendly and CMOS-compatible element. However, processes to immobilize individual Si NCs on metal electrodes are not established. The reason is that it is difficult to use the alkanedithiol molecules for immobilizing a Si NC on metal surface. This is due to the fast oxidation of the surface and the inability of the oxidized surface, which makes it difficult to form a chemical bond between Si surface and a thiol group.[23]

We propose an essential technique to immobilize Si NCs on metal surface based on electrostatic attraction. In this work, we employ boron (B) and phosphorus (P) codoped colloidal Si NCs (codoped Si NCs).[24–26] Codoped Si NCs have heavily B and P codoped shells, which induces a negative potential on the surface (ζ-potential: -42– -27 mV)[24] and prevents the agglomeration in polar solvents by the Coulomb repulsion. The perfect dispersion of NCs in solution is crucial for the self-assembly onto metal surface. The Codoped Si NCs are attached on positively charged Au surface with an amine-terminated self-assembled monolayer (SAM) by electrostatic attraction. We demonstrate the formation of a SET by placing the codoped Si NCs in the Au nanogap electrodes.

Codoped Si NCs were prepared using a method described in the previous papers.[24–26] Borophosphosilicate glass films were deposited on a stainless steel plate by co-sputtering Si, SiO_2, B_2O_3, and P_2O_5. The films were removed from the stainless steel plate and the films were crushed in a mortar. The powder was annealed in a N_2 atmosphere at 1200 °C for 30 min to grow codoped Si NCs. The annealed powder was dissolved in a hydrofluoric acid solution for 30 min in an ultrasonic bath to extract codoped Si NCs. Codoped Si NCs were centrifuged and transferred into methanol. The concentration of Si in the solution was 0.5–0.7 mg/ml. The obtained NC solution was slightly acidic (pH = 4–6).

Figure 1(a) shows a transmission electron microscope (TEM) image of codoped Si NCs. Because a negative surface potential prevents codoped Si NCs from aggregation,[24] NCs are isolated one by one and no aggregate is observed. The inset image is a high-resolution TEM (HRTEM) image of a NC. The lattice fringe corresponding to the {111} plane of Si crystal is observed.[25] Figure 1(b) shows the size distribution of codoped Si NCs obtained from the TEM images. Average diameter of NCs (D_{ave}) is 8.0 nm with a standard deviation (σ) of 2.0 nm. Note that D_{ave} can be controlled in a

a)Author to whom correspondence should be addressed. Electronic mail: kano@eedept.kobe-u.ac.jp

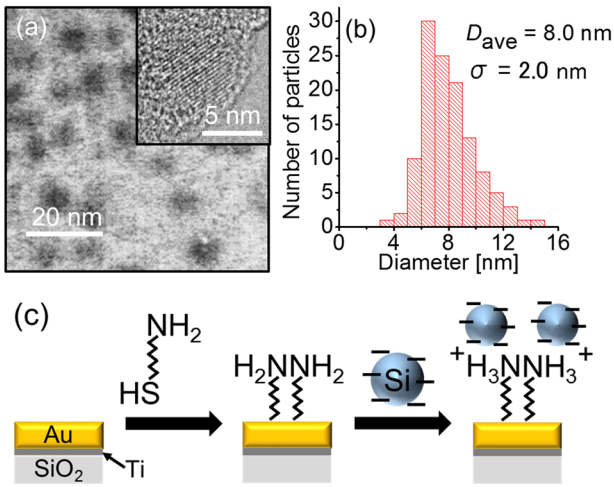

FIG. 1. (a) TEM image and (b) size distribution of Si NCs annealed at 1200 °C. Inset: HRTEM image of Si NC. (c) Schematic illustration of a method to immobilize Si NCs electrostatically on Au surface.

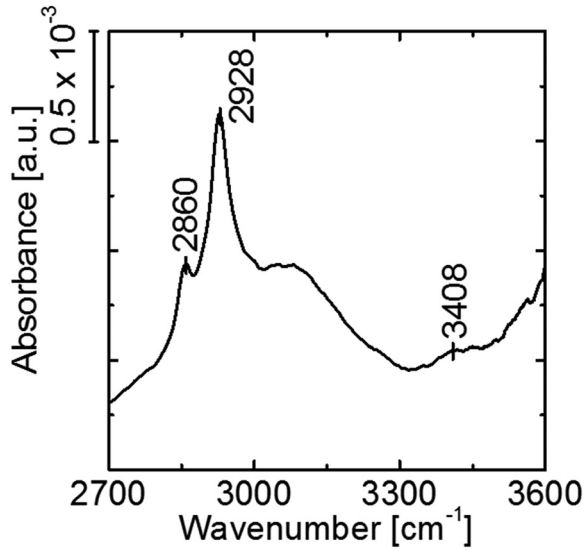

FIG. 2. IR absorption spectrum of a 6-amino-1-hexanethiol SAM on Au surface.

wide range (1–14 nm) by changing the growth temperature.[24] Irrespective of the size, codoped Si NCs have negative surface potential and thus the process can be applied to codoped Si NCs with different sizes. In this study, we chose 8.0 nm diameter NCs to make observations of individual NCs on metal electrodes by using scanning electron microscopy easier.

A self-assembly method to immobilize the codoped Si NCs on Au electrodes is described in Figure 1(c). We deposited a titanium (Ti) and Au film on a thermally oxidized SiO_2/Si substrate. After cleaning the substrate by a UV/O_3 cleaner (Samco, UV-1), the substrate was immersed in 6-amino-1-hexanethiol [$HS(CH_2)_6NH_2$, Dojindo, Japan] solution in ethanol (1 mM) for 24 h to form a self-assembled monolayer (SAM) on Au surface. Subsequently, the SAM-treated substrate was immersed in Si NC solution. The concentration of Si NC solution was diluted 1000 times by methanol. Because original Si NC solution was acidic, amino groups in a 6-amino-1-hexanethiol SAM were protonated and Au surface was positively charged in Si NC solution.[27,28] Therefore, negatively charged codoped Si NCs were attracted by Coulomb interaction and adsorbed on Au surface. Finally, the substrate was rinsed in methanol and distilled water and then dried by N_2 gas.

Figure 2 shows an infrared (IR) absorption spectrum of a 6-amino-1-hexanethiol SAM on Au surface by reflection-absorption spectroscopy measurement (PerkinElmer, Spectrum GX). In the spectrum, two prominent absorption peaks are observed at 2860 cm^{-1} and 2928 cm^{-1} assigned to the symmetric and asymmetric CH_2 stretching modes of a hydrocarbon chain, respectively.[29] A weak absorption peak at 3408 cm^{-1} is assigned to the NH stretching mode.[29] From these results, we confirmed that a 6-amino-1-hexanethiol SAM is formed on Au surface.

To confirm the validity of the method in Figure 1(c), we prepared two substrates. One is a 6-amino-1-hexanethiol SAM-treated Au substrate and the other is a bare Au substrate as a control sample. Figures 3(a) and 3(b) show the SEM (HITACHI, SU-8000) images of a 6-amino-1-hexanethiol SAM-treated Au substrate and a bare Au substrate after adsorption of Si NCs, respectively. In Figure 3(a), a large number of Si NCs represented by white spots are observed on SAM-treated Au surface. Each Si NC is well isolated even on Au surface because of electrostatic repulsion during immersion in solution. On the other hand, only a few Si NCs are adsorbed on bare Au surface. Thus, codoped Si NCs can be electrostatically adsorbed on Au surface via a 6-amino-1-hexanethiol SAM. Figure 3(c) shows a SEM image of boundary of SAM-treated Au and SiO_2 surface after immersion in Si NC solution. In contrast to SAM-treated Au surface, Si NCs are not observed on SiO_2 surface because a 6-amino-1-hexanethiol SAM is not assembled on SiO_2 surface. According to the above result, codoped Si NCs can be selectively assembled

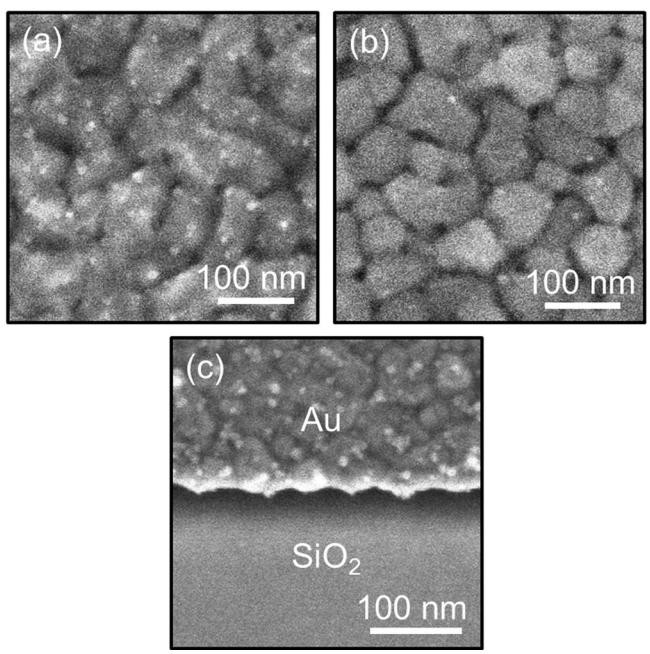

FIG. 3. (a) SEM image of a 6-amino-1-hexanethiol SAM-treated Au substrate and (b) a bare Au substrate after immersion in Si NC solution. Immersion time of both substrates was 1 h. (c) SEM image of boundary of SAM-treated Au and SiO_2 surface after immersion in Si NC solution repeatedly. Total immersion time was 4.5 h.

on Au surface by the method described in Figure 1(c). Note that a thiol group can effectively attach on many metal surface,[30] and thus, this procedure can be used for other metal surface as well as Au.

We fabricated a SET by using codoped Si NCs, a 6-amino-1-hexanethiol SAM, and electroless Au plated nanogap electrodes. Initial Ti (2 nm)/Au (10 nm) nanogap electrodes were fabricated on a Si substrate with 300-nm thermally oxidized SiO_2 by electron beam lithography and photolithography. The number of nanogap electrodes was in total 49. Initial nanogap separation between source and drain electrodes was 25 nm and two side-gate electrodes were also fabricated. Nanogap separation was reduced to the size of NCs by electroless Au plating. A detailed process of electroless Au plating was reported in a previous paper.[31] After fabrication of Au nanogap electrodes, the same adsorption process of Si NCs in Figure 1(c) was carried out.

Figure 4(a) shows a SEM image of a fabricated device and a circuit for electrical measurement. In this study, only one side-gate is used for the SET operation (the top electrode in Fig. 4(a)). Si NCs bridge between source and drain electrodes. Electrical measurements were performed by using a semiconductor parameter analyzer (Agilent, B1500) and a probe station (Nagase Techno-Engineering, GRAIL 10-LOGOS01S) in vacuum ($\sim 10^{-5}$ Pa) at 9 K. Figure 4(b) shows measured drain current–drain voltage (I_D–V_D) characteristics under applying different gate voltages $V_G = -1.92$ and 0 V. In both gate voltages, a nonlinear characteristic and a voltage range where drain current is suppressed are observed. The suppressed current region is modulated by the gate voltages; therefore, the Coulomb blockade occurs because Si NCs between the nanogap electrodes work as a Coulomb island.

Figure 5(a) shows the measured drain current–gate voltage (I_D-V_G) characteristics under applying different drain voltages. The oscillation of drain current by gate voltage (Coulomb oscillation) is clearly observed. Note that aperiodic oscillation indicates that several Si NCs work as a Coulomb island in a SET, in contrast to the periodic oscillation of a metal single-dot SET.[9] Figure 5(b) shows differential conductance (dI_D/dV_D) plotted as a function of drain voltage and gate voltage (stability diagram). The stability diagram is obtained corresponding to the Coulomb gap in I_D-V_D characteristics (Fig. 4(b)) and the peak separation of I_D-V_G characteristics (Fig. 5(a)). Measured complex stability diagram also indicates that several Si NCs are adsorbed between source and drain electrodes. Note that the rhombic shape of Coulomb diamonds guarantees a single NC working as a Coulomb island.[9] A network of dopants in NCs may cause the complex stability diagram; however, we do not have any evidence to support this assumption by now. It should be stressed here that, in the nanogap electrodes without NCs, no detectable current is observed (see supplementary material). On the other hand, with NCs, we observe SET operations in 3 nanogap electrodes out of 49. The yield is thus 6%.

Here, we roughly estimate a charging energy of single NC to confirm a validity of the operation of SET at 9 K. In

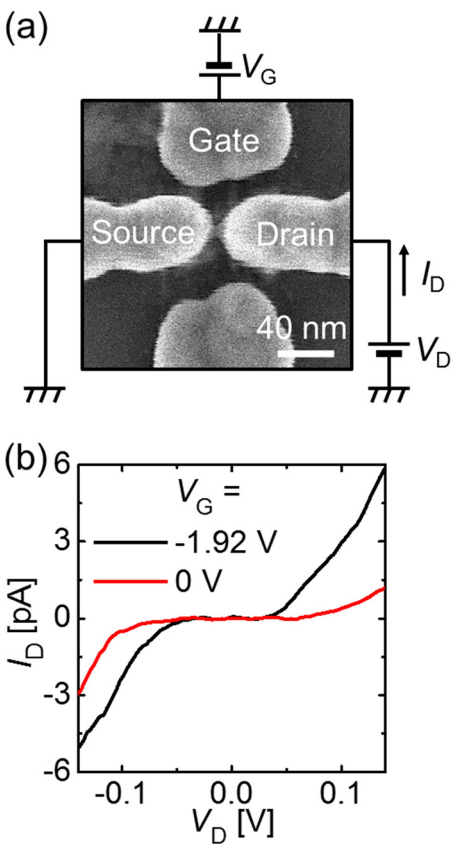

FIG. 4. (a) SEM image of a fabricated device with a circuit for electrical measurement. Immersion time of the Au nanogap electrodes in Si NC solution was 3 s. The bottom electrode in the image was not used in this work. (b) I_D–V_D characteristics of a fabricated SET under different gate voltages $V_G = -1.92$ and 0 V.

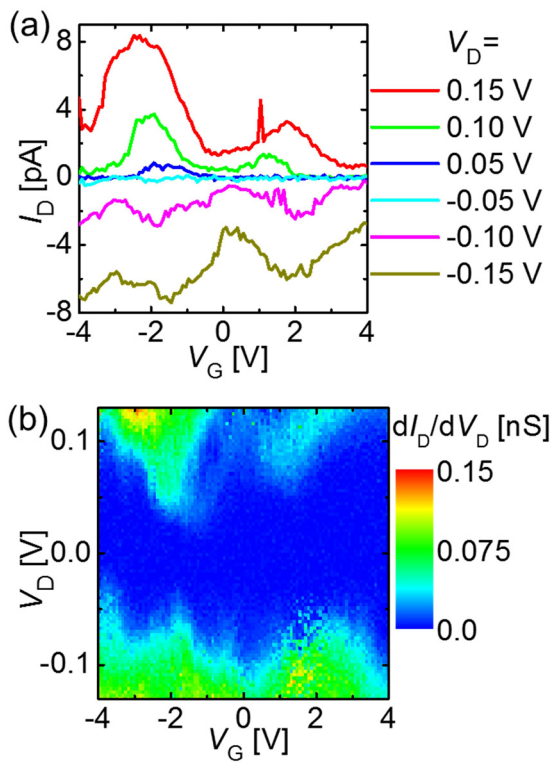

FIG. 5. (a) I_D-V_G characteristics of a fabricated SET under applying different drain voltage $V_D = 0.15$, 0.10, 0.05, −0.05, −0.10 and −0.15 V (from top to bottom). (b) Stability diagram of a fabricated SET.

the case of a SET consisting of electroless plated nanogap electrodes and a single NC, a total capacitance C_Σ is well evaluated by using a concentric sphere model[16] (i.e., a single NC is almost shielded with metal electrodes)

$$C_\Sigma = 4\pi\epsilon_0\epsilon_r \left(\frac{1}{\frac{D}{2}} - \frac{1}{\frac{D}{2}+d} \right)^{-1}, \quad (1)$$

where ϵ_0 is the permittivity of vacuum, ϵ_r is a relative permittivity of the space, D is a diameter of a NC, and d is an average distance between a single NC and metal surface. Expected total capacitance is 5.0 aF according to this concentric sphere model. In this calculation, we assume ϵ_r is a relative permittivity of the alkanethiol ($\epsilon_r = 2.6$), D is 8.0 nm, and d is a length of 6-amino-1-hexanethiol. The value of d is assumed to be 1.2 nm, which is a similar length of 1,6-hexanedithiol.[21] By calculating C_Σ in Eq. (1), we evaluate a charging energy (E_c) as $E_c = e^2/C_\Sigma$, where e is the elementary charge.[32] Evaluated E_c is 32 meV and this value is much larger than thermal energy at 9 K (0.78 meV). Therefore, an operation of a SET using codoped Si NCs ($D_{ave} = 8.0$ nm) at 9 K is reasonable.

In our previous study, the B concentration of codoped Si NCs is always larger than P concentration.[24] Analyzed by valence-band spectroscopy, the Fermi level of codoped Si NCs larger than 4 nm is close to the highest occupied molecular orbital (HOMO) level.[33] This result indicates that 8-nm codoped Si NCs are p-type semiconductor. In general, a transistor with a p-type quantum dot works in a negative gate voltage region (i.e., single-hole transistor[34,35]). However, the observed Coulomb diamond in Fig. 5(b) is in both positive and negative gate voltage regions, which is similar to that of metal NCs. A possible reason is that the Fermi level of codoped Si NCs lies among the B acceptor levels, similar to degenerate semiconductors.[36] In fact, the P and B concentrations in the present Si NCs are several at. % and about 10 at. %, respectively,[24] which are much higher than the solid solubility in Si crystal.[37] Although a majority of them are considered to be inactive and accumulated on or near the surface, it is still very plausible that the NCs are degenerate semiconductors. Unoccupied B states also exist above the Fermi level as well as thermally activated (occupied) B states, and thus, codoped Si NCs can have a similar property to metal NCs. If the size of codoped Si NCs is reduced less than 3 nm, the Fermi level approaches center of the energy gap and a typical property of a semiconductor NC is expected.

In conclusion, we developed a process to integrate colloidal Si NCs with metal surface in SETs by self-assembly. The method uses electrostatic attraction between negatively charged B and P codoped Si NCs and positively charged amine-terminated Au surface. We demonstrated the operation of the fabricated SETs at 9 K. The method developed in this work is versatile for the fabrication of different kinds of NC-based nanodevices by a bottom-up process.

See supplementary material for the current–voltage characteristics of electroless plated nanogap electrodes without Si NCs.

We would like to thank Ms. M. Miyakawa for the SEM observation and Dr. H. Sugimoto for the HRTEM observation. This work was supported by the Collaborative Research Project of Laboratory for Materials and Structures (Tokyo Institute of Technology); 2015 JST Visegrad Group (V4)-Japan Joint Research Project on Advanced Materials "NaMSeN"; Hyogo Science and Technology Association; Kyoto Technoscience Center; JSPS KAKENHI Grant No. JP16H03828; MEXT Elements Strategy Initiative to Form Core Research Center from the Ministry of Education, Culture, Sports, Science, and Technology (MEXT), Japan; and the BK Plus program, Basic Science Research program (NRF-2014R1A6A1030419).

[1]A. Zabet-Khosousi and A.-A. Dhirani, Chem. Rev. **108**, 4072 (2008).
[2]D. V. Talapin, J.-S. Lee, M. V. Kovalenko, and E. V. Shevchenko, Chem. Rev. **110**, 389 (2010).
[3]D. S. Dolzhnikov, H. Zhang, J. Jang, J. S. Son, M. G. Panthani, T. Shibata, S. Chattopadhyay, and D. V. Talapin, Science **347**, 425 (2015).
[4]J.-H. Choi, H. Wang, S. J. Oh, T. Paik, P. S. Jo, J. Sung, X. Ye, T. Zhao, B. T. Diroll, C. B. Murray, and C. R. Kagan, Science **352**, 205 (2016).
[5]J. Tang, K. W. Kemp, S. Hoogland, K. S. Jeong, H. Liu, L. Levina, M. Furukawa, X. Wang, R. Debnath, D. Cha, K. W. Chou, A. Fischer, A. Amassian, J. B. Asbury, and E. H. Sargent, Nat. Mater. **10**, 765 (2011).
[6]M. V. Kovalenko, Nat. Nanotechnol. **10**, 994 (2015).
[7]E. H. Gong, X. Yang, G. Walters, R. Comin, Z. Ning, E. Beauregard, V. Adinolfi, O. Voznyy, and E. H. Sargent, Nat. Photonics **10**, 253 (2016).
[8]F. Maier-Flaig, J. Rinck, M. Stephan, T. Bocksrocker, M. Bruns, C. Kübel, A. K. Powell, G. A. Ozin, and U. Lemmer, Nano Lett. **13**, 475 (2013).
[9]K. Maeda, N. Okabayashi, S. Kano, S. Takeshita, D. Tanaka, M. Sakamoto, T. Teranishi, and Y. Majima, ACS Nano **6**, 2798 (2012).
[10]S. K. Bose, C. P. Lawrence, Z. Liu, K. S. Makarenko, R. M. J. van Damme, H. J. Broersma, and W. G. van der Wiel, Nat. Nanotechnol. **10**, 1048 (2015).
[11]K. Horibe, T. Kodera, and S. Oda, Appl. Phys. Lett. **106**, 83111 (2015).
[12]S. Kano, Y. Azuma, D. Tanaka, M. Sakamoto, T. Teranishi, L. W. Smith, C. G. Smith, and Y. Majima, J. Appl. Phys. **114**, 223717 (2013).
[13]A. Fujiwara, K. Nishiguchi, and Y. Ono, Appl. Phys. Lett. **92**, 042102 (2008).
[14]Y. Azuma, Y. Yasutake, K. Kono, M. Kanehara, T. Teranishi, and Y. Majima, Jpn. J. Appl. Phys., Part 1 **49**, 90206 (2010).
[15]N. Okabayashi, K. Maeda, T. Muraki, D. Tanaka, M. Sakamoto, T. Teranishi, and Y. Majima, Appl. Phys. Lett. **100**, 33101 (2012).
[16]S. Kano, D. Tanaka, M. Sakamoto, T. Teranishi, and Y. Majima, Nanotechnology **26**, 45702 (2015).
[17]Y. Azuma, Y. Onuma, M. Sakamoto, T. Teranishi, and Y. Majima, Nanoscale **8**, 4720 (2016).
[18]Y. Noguchi, M. Yamamoto, H. Ishii, R. Ueda, T. Terui, K. Imazu, K. Tamada, T. Sakano, and K. Matsuda, Jpn. J. Appl. Phys., Part 1 **52**, 110102 (2013).
[19]S. Kano, Y. Azuma, K. Maeda, D. Tanaka, M. Sakamoto, T. Teranishi, L. W. Smith, C. G. Smith, and Y. Majima, ACS Nano **6**, 9972 (2012).
[20]S. Kano, T. Tada, and Y. Majima, Chem. Soc. Rev. **44**, 970 (2015).
[21]D. L. Klein, R. Roth, A. K. L. Lim, A. P. Alivisatos, and P. L. McEuen, Nature **389**, 699 (1997).
[22]M. S. Gudiksen, K. N. Maher, L. Ouyang, and H. Park, Nano Lett. **5**, 2257 (2005).
[23]S. A. Claridge, W. Liao, J. C. Thomas, Y. Zhao, H. H. Cao, S. Cheunkar, A. C. Serino, M. Andrews, and P. S. Weiss, Chem. Soc. Rev. **42**, 2725 (2013).
[24]H. Sugimoto, M. Fujii, K. Imakita, S. Hayashi, and K. Akamatsu, J. Phys. Chem. C **117**, 11850 (2013).
[25]H. Sugimoto, M. Fujii, K. Imakita, S. Hayashi, and K. Akamatsu, J. Phys. Chem. C **116**, 17969 (2012).
[26]H. Sugimoto, M. Fujii, K. Imakita, S. Hayashi, and K. Akamatsu, J. Phys. Chem. C **117**, 6807 (2013).
[27]T. Zhu, X. Fu, T. Mu, J. Wang, and Z. Liu, Langmuir **15**, 5197 (1999).
[28]F. Kuemmeth, K. I. Bolotin, S.-F. F. Shi, and D. C. Ralph, Nano Lett. **8**, 4506 (2008).
[29]N. B. Colthup, L. H. Daly, and S. E. Wiberley, *Introduction to Infrared and Raman Spectroscopy* (Academic Press, 1964).

[30]A. Ulman, Chem. Rev. **96**, 1533 (1996).
[31]V. M. Serdio, V. Y. Azuma, S. Takeshita, T. Muraki, T. Teranishi, and Y. Majima, Nanoscale **4**, 7161 (2012).
[32]L. P. Kouwenhoven, N. C. van der Vaart, A. T. Johnson, W. Kool, C. J. P. M. Harmans, J. G. Williamson, A. A. M. Staring, and C. T. Foxon, Z. Phys. B **85**, 367 (1991).
[33]Y. Hori, S. Kano, H. Sugimoto, K. Imakita, and M. Fujii, Nano Lett. **16**, 2615 (2016).
[34]S. Lee, K. Miyaji, M. Kobayashi, and T. Hiramoto, Appl. Phys. Lett. **92**, 73502 (2008).
[35]J. Llobet, E. Krali, C. Wang, J. Arbiol, M. E. Jones, F. Perez-Murano, and Z. A. K. Durrani, Appl. Phys. Lett. **107**, 223501 (2015).
[36]D. Mocatta, G. Cohen, J. Schattner, O. Millo, E. Rabani, and U. Banin, Science **332**, 77 (2011).
[37]S. M. Sze, *Physics of Semiconductor Devices*, 2nd ed. (Wiley, New York, 1981).